Geosynthetics - 7th ICG - Delmas, Gourc & Girard (eds) © 2002 Swets & Zeitlinger, Lisse ISBN 90 5809 523 1

Analytical modeling and field performance testing of geocomposite membrane in flexible pavement systems

I.L. AL-QADI & M.A. ELSEIFI, Virginia Tech, Blacksburg, VA, USA

ABSTRACT: Two sections at the Virginia Smart Road were instrumented and constructed to quantify the effectiveness of a geocomposite membrane as a moisture barrier and as a strain energy absorber. Results of ground penetrating radar (GPR) surveys and time domain reflectometer (TDR) moisture sensors validated the effectiveness of the geocomposite membrane in abating water infiltration into the subbase layer even in the event of heavy rain. The potential of the geocomposite membrane to mitigate the reflection of cracks was theoretically investigated using the finite element (FE) analysis approach. A model was developed to simulate a cracked pavement structure by creating a singularity at the crack tip. Four contour lines were simulated around the crack to calculate the path-independent integral. Analysis of results indicates that the geocomposite membrane is effective in dissipating a large amount of energy around the cracked region. This has been verified by field cores and falling weight deflectometer (FWD) data analyses. The study showed that a soft interlayer system might increase the number of cycles for crack initiation by several orders of magnitude.

1 INTRODUCTION

Traditional materials have performed satisfactorily on a wide range of roads in the past; however, recent failures have attracted the attention of the public and media to the current status of the transportation infrastructure. According to the 2001 ASCE report, $94 billion a year is needed over the next 20 years to fix the US highway and bridge system. This is a direct result of the continuous increase of traffic and axle loads. To rehabilitate and maintain the crumbling transportation infrastructure, new materials and construction techniques have been recently introduced. Among the new materials utilized to improve pavement and bridge deck performance are geosynthetics. To accurately quantify the benefits of geosynthetics to flexible pavement systems, a better understanding of the contributing mechanisms is necessary. This can only be achieved by linking field performance to well-established engineering theories. This paper illustrates how the link between experimental and theoretical observations can be established to evaluate the effectiveness of a specially designed geocomposite membrane system to act as a moisture barrier and as a strain energy absorber. The experimental results presented in this study were obtained based on falling weight deflectometer (FWD) testing and environmental monitoring conducted at the heavily instrumented Virginia Smart Road (Al-Qadi et al. 2001).

The Virginia Smart Road offers an opportunity to explore the effectiveness of a specially designed geocomposite membrane as a moisture barrier and as a strain energy absorber. The geocomposite membrane, consisting of a 2-mm-thick low modulus polyvinyl chloride (PVC) backed on both sides with 150g/m^2 polyester nonwoven geotextile, was installed in two different sections at the Virginia Smart Road. In section J, the geocomposite membrane was installed underneath an asphalt-treated drainage layer to test its effectiveness as a moisture barrier. In section K, the geocomposite membrane was installed within the hot-mix asphalt (HMA) base to investigate its capability to relieve excessive strain energy; a schematic of the layered system of each section is presented in Figure 1 (all designations are in accordance with the Virginia Department of Transportation specifications).

While this geocomposite membrane has been used on two bridge decks in Italy, it has never been used on any roads or bridges in the United States prior to its installation at the Virginia Smart Road pavement test facility. In 2001, it was installed on a small bridge deck in Delaware.

2 OPTIMUM TACK COAT RATE

Prior to the installation of the geocomposite membrane, an experimental program was conducted to determine the optimum asphalt binder tack coat application rate needed in the field (Donovan et al. 2000). This testing simulated the slippage that may occur at the geocomposite membrane interface by applying a cyclic constant shear loading to a geocomposite membrane sandwiched between two pavement layer materials (see Figure 2).

To evaluate the optimum tack coat application rate, the number of cycles required to cause shear failure at the interface was measured using a servo-hydraulic testing machine. Results of the experimental program indicated that the optimum tack coat rate is 1.40kg/m^2 between the geocomposite membrane and the base HMA layer, and 1.50kg/m^2 between the geocomposite membrane and the surface HMA.

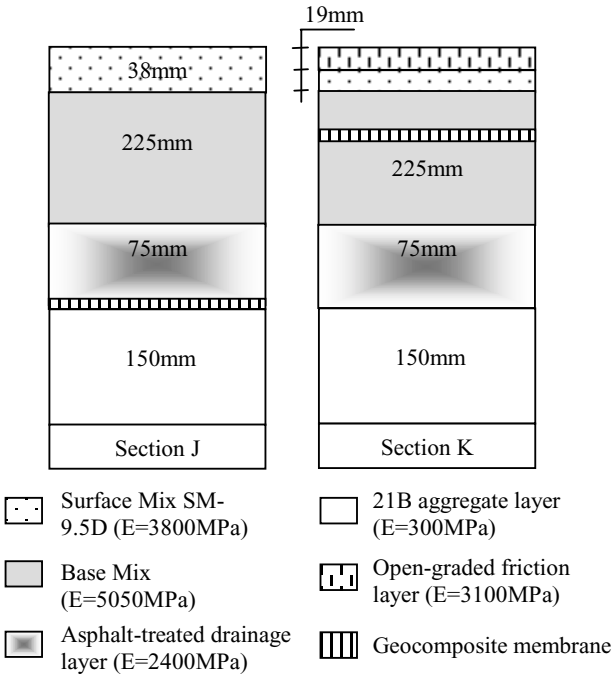

Figure 1. Pavement design (section J and K).

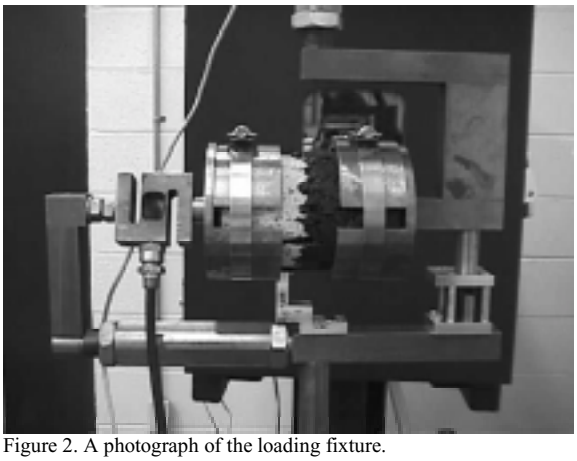

Figure 2. A photograph of the loading fixture.

3 GEOCOMPOSITE INSTALLATION

Prior to installation, the area to be covered with geocomposite membrane was carefully cleaned of any loose aggregates. The installation of the geocomposite membrane in section J (moisture barrier over a granular material) did not necessitate the use of a prime coat between the geotextile and the underneath layer (21B aggregate subbase layer). A prime coat may not be effective when applied to a granular material (e.g. 21B) due to the nature of the surface, which accumulates a large amount of loose aggregates and due to the fact that greater friction may exist between the geocomposite membrane and the aggregate layer when the prime coat is absent.

Transverse joints between PVC rolls were staggered to prevent the creation of a weak joint across the pavement lane. At the longitudinal joints, a 55mm-length weld was performed by applying hot air to melt the uncovered PVC end. The welding was then carefully checked. Figure 3 illustrates the final product of the installation. The upper surface of the geocomposite membrane was primed using PG 64-22 asphalt binder at an application rate of 1.45kg/m^2. Seventy-five mm of asphalt treated open-graded drainage layer (OGDL) was then placed on top of the geocomposite membrane. Sudden application of truck brakes during installation of the upper layer was avoided to prevent the wrinkling of the geocomposite membrane. Temperature and moisture sensors were placed on both sides of the geocomposite membrane, while three pressure cells were installed under the geocomposite membrane.

The installation of the geocomposite membrane in section K was slightly different than the previous procedure; it was installed after placing two lifts of BM-25.0 HMA base. After the installation of the geocomposite membrane on the tack coated layer and prior to applying the tack coat above it, a pneumatic-tired roller (PTR) was used to compact the geocomposite membrane to ensure good adhesion between the geocomposite membrane and the underneath layer. Another lift of BM-25.0 was then placed followed by 19-mm-thick SM 9.5D and the open-graded friction course (OGFC) layer.

Figure 3. Geocomposite membrane before prime coat application.

To verify the effect of the tack coat application rate, two rates were applied at the Virginia Smart Road when the geocomposite membrane was installed in section K: one at the optimum HMA base rate and one at 0.2kg/m^2 above the optimum HMA base rate. Figure 4 presents two cores extracted from two different locations in section K that have different tack coat application rate. Core A, which has the optimum tack coat application rate, was intact after extraction, while Core B with just 0.2kg/m^2 above the optimum tack coat application rate showed weak bonding between the geocomposite membrane and the underneath HMA layer.

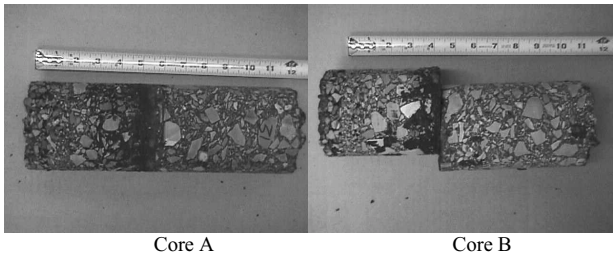

Core A Core B

Figure 4. Extracted cores from the Virginia Smart Road.

4 MOISTURE BARRIER EVALUATION

Evaluation of the geocomposite membrane effectiveness as a moisture barrier was based on ground penetrating radar (GPR) surveys, and continuous moisture monitoring using time-domain reflectometry (TDR) (Elseifi et al. 2001). Based on a qualitative

simplified approach (Al-Qadi et al. 2001), different GPR scans taken for two sections (with and without geocomposite membrane) were compared. Figure 5 illustrates a scan taken at the pavement surface of section J (with geocomposite membrane). In this scan, the uniformity of the color refers to the absence of any abnormal spots (i.e. water accumulation, voids, etc.). It is clear from this figure that water did not accumulate in the overlying layers (e.g. OGDL) prior to lateral drainage. It is thought that accumulation of the water in the overlying layers may only occur if the layer lateral slopes are not adequately designed. The lateral slope is 2% at the Virginia Smart Road

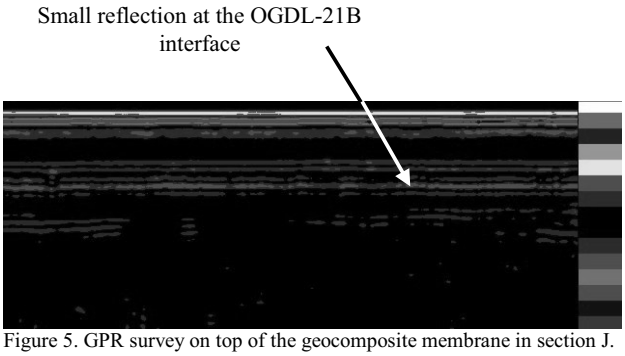

Figure 5. GPR survey on top of the geocomposite membrane in section J.

Conversely, Figure 6 presents a scan taken for a similar pavement section, but without the geocomposite membrane. As is obvious in this case, a large reflection due to moisture presence (shown by an arrow) appears at the interface between the OGDL and the underneath layer (21B aggregate layer). This indicates that the 21B layer has high moisture content, which may not be desirable as it may reduce the resilient modulus of that layer and, hence, the structural capacity of the pavement system.

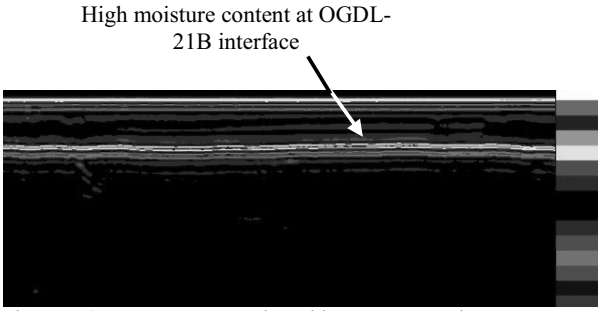

Figure 6. GPR survey on a section without geocomposite.

Subbase and subgrade moisture contents were measured using time domain reflectometers (TDRs). Two types of TDR probes were used at the Virginia Smart Road: the traditional CS610 (three-rod probe) and the newly developed CS615 (two-rod probe). Calibration models were used to analyze the TDR collected data (Diefenderfer et al. 2000). Two sections with and without geocomposite membrane were compared. Figure 7 shows the collected data for three CS615 probes in the 21B aggregate layer of sections B and J along with the precipitation occurring over the same period of time. As noticed from this figure, the measured moisture content in the 21B aggregate layer in section B is highly dependent on the amount of precipitation received. For instance, a large increase in volumetric moisture content (around 8%) occurred on this section after the rain event of August 28, 2000. In contrast, the moisture content in section J remained nearly constant over the entire monitored period. Even after the high rain event of August 28, 2000, the measured volumetric moisture content in the 21B aggregate layer remained at the same level. The same trend was also observed in section K. This indicates the effectiveness of the geocomposite membrane in maintaining constant volumetric moisture content of the underneath layers over different precipitation periods.

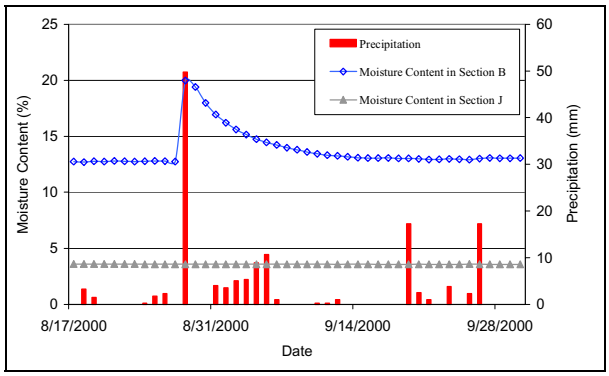

Figure 7. Volumetric moisture content measurements in sections B and J along with the precipitation occurring over the same period of time.

5 STRAIN ENERGY ABSORPTION EVALUATION

The evaluation of the strain energy absorption capabilities of the geocomposite membrane was investigated utilizing FWD measurements at the Virginia Smart Road and theoretical finite element (FE). A two-dimensional (2D) FE model was created to investigate the crack initiation and propagation in a typical three-layer flexible pavement system.

Two distinct phases were considered in the reflection of the crack process:

- The crack initiation phase represents the position of the crack just underneath the interlayer system. As presented in this study, this is the perfect position for a strain-energy reliever system to delay the reflection of cracks by 'protecting' the crack tip from the excess of energy. The number of cycles of a specific load a pavement can withstand before it cracks may be related to the critical shear strain (Vanelstraete et al. 2000):

$$N = 4.856x10^{-14}\varepsilon_{zx}^{-4.76} \quad (1)$$

where N = number of cycles before crack initiation; and ε_{zx} = shear strain 10mm above the crack tip.

- The crack propagation phase represents the case where the crack passes through the interlayer system propagating to the surface.

To better understand the mechanism of both cases, the commercial software ABAQUS version 5.8-1 was used for the FE modeling of the pavement structure (ABAQUS 1998). The developed FE code represents a typical flexible pavement overlay application; an existing pavement structure consists of a 127mm cracked HMA layer and a 203mm base layer. A HMA overlay is applied to the cracked HMA with variable thicknesses.

All layers were assumed fully bonded except the surface interaction between the base and subgrade layers, which was assumed to be a friction-type contact (Mohr-Coulomb theory). This assumption is based on the fact that when granular surfaces are in contact, they usually transmit shear as well as normal forces across their boundary. Small sliding was also allowed between the aggregate layers.

To investigate the geocomposite membrane effectiveness, two models were developed, one incorporating the geocomposite membrane between the cracked HMA layer and the overlay, and the second with the overlay applied directly on top of the HMA as a base of comparison. All materials were considered linear elastic with respective moduli shown in Table 1 for the different investigated cases.

Table 1. Overview of the investigated cases.

Layer	Case 1	Case 2	Case 3
Case ID	A	B	C
Overlay Thickness (mm)	50.8	76.2	101.6
Overlay Modulus (MPa)	4135	4135	4135
HMA Modulus (MPa)	2415	2415	2415
Base Modulus (MPa)	240	240	240
Subgrade Modulus (MPa)	70	70	70

The dimension of the modeled portion is 2260mm x 420mm. These dimensions were selected to reduce any edge effect errors, while keeping the elements' sizes within acceptable limits (modeling constraints). The generated mesh distribution was designed to give an optimal accuracy (small elements around the crack and large elements far from the crack). While 6.25mm elements were used in the region close to the crack, 12.5mm elements were used in the regions far from the crack. All elements were 8-nodes biquadratic (CPE8R) to improve the level of accuracy. Due to the large number of degrees of freedom (22000), reduced integration elements were selected to increase the rate of convergence. All layers were simulated with the same shape to preserve the continuity of nodes between consecutive layers. In total, 3,800 elements were needed to simulate this problem. ABAQUS generated an additional 263 contact elements to simulate contact between the layers. Infinite elements (CINPE5R) were used to simulate the far-field region in the model. This type of element is useful in eliminating edge effect errors when the region of interest is small in size compared to the surrounding medium. Figures 8 and 9 illustrate the general layout of the developed model.

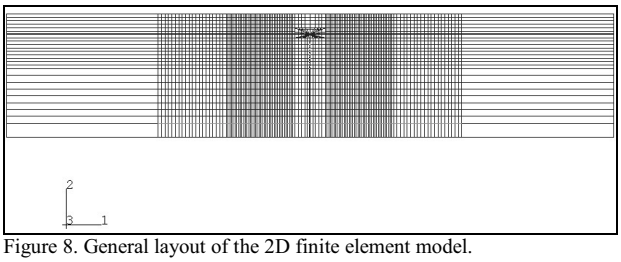

Figure 8. General layout of the 2D finite element model.

Elastic element foundations were used to simulate the support provided by the subgrade to the pavement structure. These elements, which act as nonlinear springs to the ground, provide a simple way of including the stiffness effects of the subgrade without fixation of nodes at the bottom of the model. Due to the axisymmetric position of the crack with respect to the load, a full model was developed. A static single tire load (26kN) was assumed with a uniform pressure of 724kPa applied over a circular area.

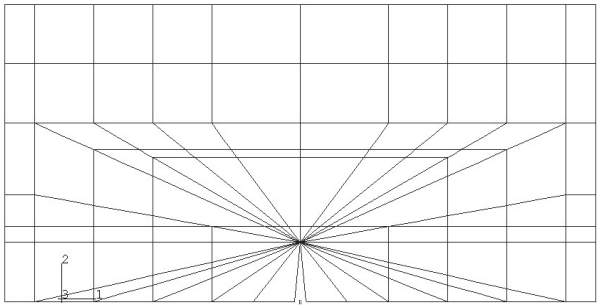

Figure 9. Illustration of the cracked region in the developed model.

5.1 *Crack Simulation and Creation of the Singularity*

A crack was induced in the existing HMA layer (see Figure 10). The crack location was selected based on the expected shear stress distribution with the distance from the load. Due to the symmetry, the critical shear stress should occur at the edge of the load, and not at the center. To create the singularity at the crack tip, a focused mesh was developed (see Figure 9). The major advantage of this technique is that a crack is present at the location of the singularity, and thus stresses around the crack tip may be calculated based on this fact. This is not the case with ordinary finite element models with fine meshes. To create a singularity of order $r^{1/2}$, the mid-side nodes along the sides of the cracks are moved to the quarter positions next to the crack tip. To validate the singularity, all elements around the crack tip must be quadratic elements, and then 'collapsed' to form triangular elements. This focused mesh allows for evaluation of the path independent J-integral through different contour lines (four contour lines are shown in Figure 10). The J-integral is defined as the change in mechanical energy per unit area of new crack surface (Rice 1968):

$$J = \int_{\Gamma} \left(U dy - T \frac{\partial u}{\partial x} ds \right) \quad (2)$$

where Γ = a curve that surrounds the crack tip; U = strain energy density; y = direction normal to the crack line; T = traction vector; u = displacement vector; and ds = differential element of arc Γ.

For linear elastic materials, and for elastoplastic materials (when unloading does not occur), the J-integral should be path independent. This allows the characterization of discontinuities of stresses or strains (at the singularity) from results obtained at some distance from the discontinuity (Andruet 1998). The accuracy of the results may then be checked by calculating the J-integral for several contour (path) lines. ABAQUS uses a domain integral technique to calculate the J-integral. Numerical tests suggest that the results of the first contour line do not provide a high accuracy, therefore only the results of three contour lines were considered. Variations in the calculated J-integral were minimal with a coefficient of variation (CV) ranging between 2.5% to 3.5% for the different overlay thicknesses. The path independent J-integral was calculated at different locations of the crack to study the geocomposite membrane effects on both the crack initiation and propagation phase.

5.2 *Model Results and Analyses*

5.2.1 *Crack Initiation Phase*

Figure 10 illustrates the calculated shear strain for each of the investigated cases (see Table 1). As shown in this figure, the geocomposite membrane clearly reduces the shear strain at the bottom of the overlay. This contribution is valid for all thicknesses of overlay.

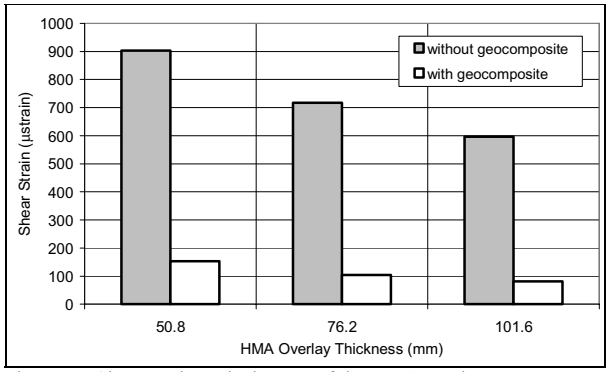

Figure 10. Shear strain at the bottom of the HMA overlay.

Based on Equation 1, Figure 11 illustrates the computed number of cycles that the overlay is able to withstand before crack initiation in a semi-logarithmic scale. As illustrated in this figure, the improvement introduced by the geocomposite membrane is of several orders of magnitude.

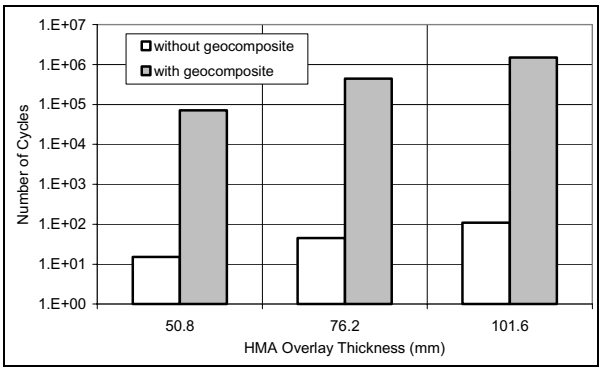

Figure 11. Number of cycles for crack initiation for the cases with and without geocomposite membrane.

The ability of the geocomposite to reduce the shear strain at the bottom of the overlay (as well as other straining actions) is based on the fact that it can dissipate most of the energy generated at the crack tip due to the singularity. This dissipation characteristics is governed by two major factors:

- The softer the interlayer, the more deformation it can exhibit based on the crack state of stresses, and therefore the more energy it can dissipate.
- The exhibited deformation should be within the elastic limits of the interlayer. An elastomeric interlayer system (soft interlayer, or stress absorbing membrane interlayer [SAMI]) would best fit this application.

To quantify this energy dissipation concept, the work (strain energy per unit volume) was calculated at the bottom of the overlay, and within the geocomposite membrane using the following equation:

$$W_v = 0.5(\sigma_1 e_1 + \sigma_2 e_2) \quad (3)$$

where W_v = strain energy per unit volume; and σ and e = principal stresses and strains in 2D.

It is useful to remember that the more energy available at a specific location, the more energy dissipation required at this location through deformation or crack initiation. Using Equation 3, Figure 12 shows the amount of strain energy per unit volume stored within the geocomposite membrane, and at the bottom of the overlay (with and without geocomposite membrane) in a semi-logarithmic scale. As shown in this figure, more energy is available at the bottom of the overlay when the geocomposite is absent. It is also clear that a significant amount of energy is stored within the geocomposite, and this will be dissipated through deformation of the soft interlayer. However, it is important to realize that the stored energy will be dissipated through deformation only if it remains within the elastic range of the interlayer. For the considered geocomposite membrane, a maximum elongation of 100% is allowed within the elastic range of the interlayer. For a given interlayer, the elastic limit may eventually depend on the thickness and the modulus of elasticity of the material (The modulus of elasticity for the geocomposite membrane was assumed 7 MPa, and the thickness was 2.5mm).

5.2.2 *Crack Propagation Phase*

Propagation of the crack was investigated through the evaluation of the path independent J-integral for different locations of the crack within the HMA overlay for Case 2 (see Table 1). All the considered locations assumed that the crack passed through the geocomposite membrane and is propagating vertically to the top. Figure 13 shows the variation of the J-integral as the crack propagates vertically to the top. As shown in this figure, the pavement without geocomposite membrane is less favorable to the propagation of the crack than the pavement with geocomposite membrane given that the crack passes through the interlayer system. This can be explained by the reduced stiffness of the pavement with geocomposite membrane as compared to the pavement without geocomposite membrane. In addition, two factors should be recognized:

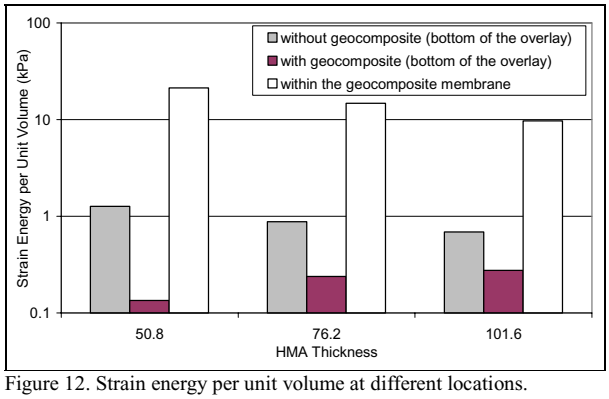

Figure 12. Strain energy per unit volume at different locations.

- This analysis assumes that the crack propagates vertically through the geocomposite membrane. This may not be the case in real pavement, as presented in the following section, which shows that the crack never propagates through the soft interlayer.
- The calculated shear strain with the geocomposite membrane is so small (see Figure 10) that this propagation mechanism (Mode II, shearing mode of the crack tip) may not mobilize enough energy to be effective to propagate a crack through the interlayer system.

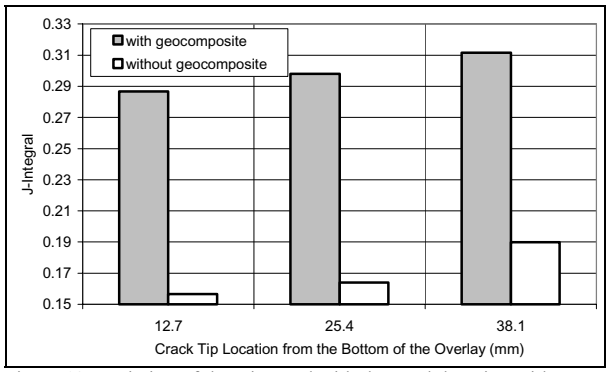

Figure 13. Variation of the J-integral with the crack location with respect to the bottom of the overlay.

5.3 *Experimental Observations and Interpretations*

Figure 14 illustrates the performance of the geocomposite membrane in delaying the reflection of cracks when installed in a bridge deck in Italy (1997). This picture was taken by the principal author during a visit to the bridge in 1999. As shown in this figure, the crack did not propagate through the geocomposite membrane, but completely stopped at the interlayer level.

Based on the results of this study, the mechanism of crack initiation and propagation when a strain energy absorption interlayer is used can be summarized as follows:

1. Due to traffic and thermal loading, an existing crack moves horizontally (due to the Poisson's effect and horizontal loading) and vertically (due to shear loading). Due to the low stiffness of the geocomposite membrane, most of the available energy is dissipated by deformation taking place within

the interlayer (see Figure 12). Hence, the crack would probably stop at this level, and the only damage that may occur is debonding between the geocomposite membrane and the existing pavement.

2. As suggested in previous work by Lytton (1989), the crack may re-initiate at the bottom of the overlay. However, the calculated shear strain at the bottom of the overlay indicates that the required number of cycles for the crack to initiate is extremely high when the geocomposite membrane is used. Based on these results, it is clear that the geocomposite membrane diminishes the potential of an existing crack to reflect in a HMA overlay given that it has the appropriate thickness and properties. However, other modes of failure (such as fatigue of the overlay) should not be ignored or overlooked.

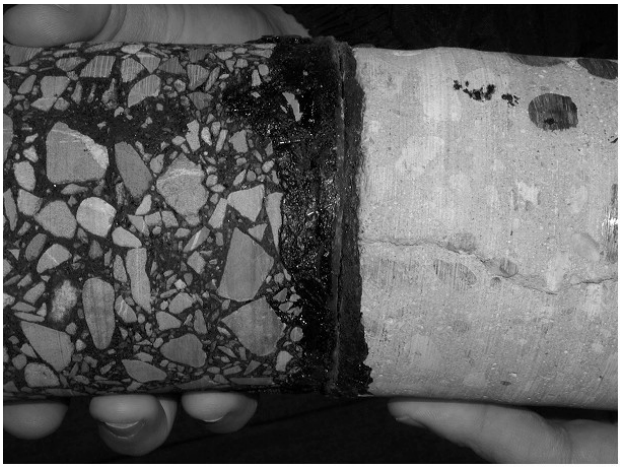

Figure 14. Performance of the geocomposite membrane in delaying the reflection of cracks in a bridge deck in Italy.

From the previous analysis, it is clear that the geocomposite membrane is not providing any types of reinforcement to the pavement. In contrast, the geocomposite membrane makes the pavement more flexible, and therefore softer. It is expected that a pavement with a soft interlayer would exhibit more vertical and horizontal deformations than a similar pavement without the geocomposite membrane. Falling weight deflectometer measurements at the Virginia Smart Road confirmed this hypothesis. Figure 15 illustrates the measured deflection directly above and below the geocomposite membrane in section J. As shown in this figure, the center deflection exhibits a very high jump due to the polymeric nature of the membrane. The same trend was observed in the FE calculated vertical deflection for a centered load. Therefore, such deformation should be considered when geocomposite membrane is used.

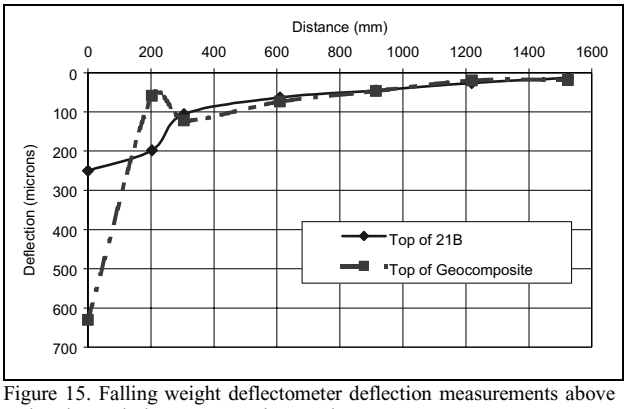

Figure 15. Falling weight deflectometer deflection measurements above and underneath the geocomposite membrane.

6 CONCLUSIONS

Based on this study, the following conclusions may be drawn:

- Ground penetrating radar surveys and continuous moisture monitoring using time domain reflectometry indicate the effectiveness of the specially designed geocomposite membrane in abating the moisture penetrating into the underneath layers.
- When used in rehabilitation applications, a geocomposite membrane is able to dissipate most of the available energy at the crack tip, and therefore it diminishes the potential of an existing crack to reflect into the overlay given that it has the appropriate thickness and properties.
- When used as a strain energy absorber, a geocomposite membrane reduces the crack initiation potential by several times, and thus may significantly increase the pavement service life.
- The effectiveness of the geocomposite membrane as a moisture barrier and as a strain energy absorber offers the potential to use this type of interlayer as a multi-purpose system. The effect of potential stripping in HMA or excessive deflection should be considered based on the pavement structure and/or the geocomposite membrane material and thickness used.

7 ACKNOWLEDGEMENTS

The authors acknowledge the support by the Virginia Center for Innovative Technology, Virginia Transportation Research Council, Virginia Department of Transportation, Carpi USA, and Atlantic Construction Fabrics. The authors would like to recognize the assistance of A. Loulizi, S. Case, D. Leonard, E. Donovan, B. Diefenderfer, G. Flintsch, S. Lahouar, T. Freeman, A. Appea, J. Wilkes, K. Light, R. Orren, and K. Taylor.

REFERENCES

"ABAQUS, Finite element computer program." 1998. Version 5.8, Hibbitt, Karlsson and Sorensen, Inc, MI.

Al-Qadi, I. L., Flintsch, G. W., Loulizi, A., Lahouar, S., and Nassar, W. 2001. Pavement instrumentation at the Virginia Smart Road. 14th IRF Road World Congress, Paris, France.

Al-Qadi, I. L., Loulizi, A., and Lahouar, S. 2000. GPR calibration at the Virginia Smart Road. GPR 2000, Proceedings of the 8th International Conference on Ground Penetrating Radar, D. A. Noon, G. F. Stickley, and D. Longstaff, Eds., SPIE Vol. 4084, Gold Cost, Queensland, Australia: 176-181.

Andruet, R. H. 1998. Special 2-D and 3-D geometrically nonlinear finite elements for analysis of adhesively bonded joints. PhD. Thesis, Virginia Tech, Blacksburg, VA.

Diefenderfer, B. K., Al-Qadi, I. L., and Loulizi, A. 2000. Laboratory calibration and field verification of soil moisture content using time-domain reflectometry. *Transportation Research Record*, 1699, TRB, National Research Council, Washington, D.C.: 142-150.

Donovan, E. P., Al-Qadi, I. L., and Loulizi, A. 2000. Optimization of tack coat application rate for a geocomposite membrane used on bridge decks. *Transportation Research Record*, 1740, TRB, National Research Council, Washington, D.C.: 143-150.

Elseifi, M.A., Al-Qadi, I.L., Loulizi, A., and Wilkes, J. 2001. Performance of a geocomposite membrane as a pavement moisture barrier. Paper No. 01-2660 presented and accepted for publication to transportation research board 80th annual meeting, National Research Council, Washington, D.C.

Lytton, R. L. 1989. Use of geotextiles for reinforcement and strain relief in asphalt concrete. *Geotextiles and Geomembranes*, Vol. 8: 217-237.

Rice, J. R. 1968. Mathematical analysis in the mechanics of fracture. *Fracture-An Advanced Treatise*, Vol. II, Academic, New York: 191-308.

Vanelstraete, A., D. Leonard, and Veys, J. 2000. Structural design of roads with steel reinforcing nettings. *Proceedings of the 4th International RILEM Conference – Reflective Cracking in Pavements*, E & FN Spon: 56-67.